The Structure of the MAP2K MEK6 Reveals an Autoinhibitory Dimer

Xiaoshan Min,[1,4] Radha Akella,[1] Haixia He,[1] John M. Humphreys,[1] Susan E. Tsutakawa,[2] Seung-Jae Lee,[1] John A. Tainer,[2]
Melanie H. Cobb,[3] and Elizabeth J. Goldsmith[1,*]

1Department of Biochemistry, The University of Texas Southwestern Medical Center at Dallas, 5323 Harry Hines Boulevard, Dallas,
TX 75390-8816, USA
2Lawrence Berkeley National Lab, 1 Cyclotron Road, Berkeley, CA 94720, USA
3Department of Pharmacology, The University of Texas Southwestern Medical Center at Dallas, 5323 Harry Hines Boulevard, Dallas,
TX 75390-9041, USA
4Present address: Amgen, One Amgen Center Drive, Thousand Oaks, CA 91320-1799, USA
*Correspondence: elizabeth.goldsmith@utsouthwestern.edu

SUMMARY
MAP2Ks are dual-specificity protein kinases functioning at the center of three-tiered MAP kinase modules. The structure of the kinase domain of the MAP2K MEK6 with phosphorylation site mimetic aspartic acid mutations (MEK6/DN/DD) has been solved at 2.3 A° resolution. The structure reveals an autoinhibited elongated ellipsoidal dimer. The enzyme adopts an inactive conformation, based upon structural queues, despite the phosphomimetic mutations. Gel filtration and small-angle X-ray scattering analysis confirm that the crystallographically observed ellipsoidal dimer is a feature of MEK6/DN/ DD and full-length unphosphorylated wild-type MEK6 in solution. The interface includes the phosphate binding ribbon of each subunit, part of the activation loop, and a rare ‘‘arginine stack’’ between symmetry-related arginine residues in the N-terminal lobe. The autoinhibited structure likely confers specificity on active MAP2Ks. The dimer may also serve the function in unphosphorylated MEK6 of preventing activation loop phosphorylation by inappropriate kinases.

INTRODUCTION

MAP kinase modules are three-tiered kinase cascades that confer switch-like responses to extracellular and stress stimuli in eukaryotes. The modules induce changes in cell program and cell fate in processes such as differentiation, transformation, apoptosis, and senescence (Chen et al., 2001; Deng et al., 2004; Johnson and Lapadat, 2002; Pearson et al., 2001). MAP kinase modules are chemically interesting because the central MAP kinase kinases (MEKs) are dual specificity, phosphorylating a Tyr and then a Ser/Thr residue to activate the MAP kinase (Haystead et al., 1992). They are physically interesting because there are numerous distinct MAP kinase modules which must maintain pathway specificity. Of over a dozen MAP kinases in the human genome, two of the best studied are the extracellular signal-regulated kinase 1/2 (ERK1/2) and its activators MAP/ ERK kinases 1 and 2 (MEK1/2), and p38 MAP kinase isoforms and their activators MEK6 and MEK3 (Raman et al., 2007). Other well-studied pathways include the c-Jun N-terminal kinases (JNKs) activated by MEK4 and MEK7, and ERK5 (Chen et al., 2001), which is activated by MEK5. ERK1/2 are activated by mitogens and growth factors (Raman et al., 2007; Yoon and Seger, 2006). In contrast, p38 isoforms and MEK6 are activated by bacterial liposaccharides, interleukins, tumor necrosis factor, and cellular stresses such as osmotic shock and UV radiation (Zarubin and Han, 2005). ERK5 and MEK5 appear to be activated by a mixture of these signals (Wang and Tournier, 2006). Not surprisingly, MAP kinase module components are drug targets for several classes of diseases, including cancer, inflammation, and degenerative diseases (Sebolt-Leopold and English, 2006).

How pathway fidelity is maintained in MAP kinase modules is being intensively studied, and is now known to involve a variety of docking and scaffolding interactions (Raman et al., 2007; Tanoue and Nishida, 2003). Especially relevant to the present study, it has been shown that docking motifs (D motifs) in the N termini of MAP2Ks bind to MAPKs (Bardwell et al., 2003; Bardwell, 2006). Further, a docking sequence in the C terminus of MAP2Ks has been shown to mediate interactions with MAP3Ks (Takekawa et al., 2005). This motif has been termed the DVD motif, and in MEK6 encompasses the last 23 residues. Thus, mammalian MAP2Ks bind both downstream MAPKs and upstream MAP3Ks through docking interactions.

Structural data on MAP kinases are relatively abundant (Goldsmith et al., 2007); structures of full-length inactive and active forms of ERK2, p38 isoforms, and JNK isoforms reveal how MAP kinases are activated by activation loop phosphorylation (Bellon et al., 1999; Canagarajah et al., 1997; Wang et al., 1997; Xie et al., 1998; Zhang et al., 1994). How docking interactions are mediated in MAP kinases has also been studied (Chang et al., 2002; Heo et al., 2004; Liu et al., 2006; Remenyi et al., 2005; Zhou et al., 2006). Docking interactions both engage partners and induce conformational changes that increase activation loop accessibility. These conformational changes are likely to contribute to pathway fidelity, because only kinases and phosphatases that have the right docking motif can unlock the activation loop for chemistry. Structures are also available for MAP3Ks that reveal some aspects of their regulation by autoinhibition and activation loop phosphorylation. These include the kinase domain structures of B-Raf and TAO2 (Wan et al., 2004; Zhou et al., 2004), and the RAS binding domain of B-Raf (Nassar et al., 1995).

Despite the intrinsic interest in MAP2Ks as dual-specificity kinases assuming a central role in MAP kinase modules, only one structural study has been reported, on the ERK2 activators MEK1/2 (Ohren et al., 2004). To find a fragment that would crystallize, Ohren et al. made an N-terminal truncation eliminating the MAPK binding D motif. The structures observed were unphosphorylated and inhibitor bound and clearly inactive (discussed below). The MEK1/2 structures also revealed an unexpected dimer. To learn more about the anatomy and regulation of MAP2Ks, in this study we have determined the structure of the MAP2K MEK6, one of the major activators of the p38a MAP kinase (Han et al., 1996). Following the protocol of Ohren et al., we made an N-terminal truncation mutant deleting the D motif.

Further, we mutated the two phosphorylation sites of MEK6, Ser207 and Thr211, to aspartic acid to mimic phosphorylation (MEK6/DN/DD), in hopes of seeing the active form of a MAP2K.

However, the structure of this mutant reveals a novel autoinhibitory dimer, despite the activating point mutations. The active site is completely blocked in the dimer, and the activation loop is also sequestered in the interface. Small-angle X-ray scattering (SAXS) analysis and gel filtration reveal that dimers are formed by MEK6/ DN/DD and wild-type MEK6. We propose that the dimer interaction presents a mechanism for regulation of both the activity and activation of MEK6.

RESULTS

The construct used for crystallography in this study, MEK6/DN/ DD (residues 45–334 of MEK6), contains two phosphorylation mimetic mutations in the activation loop (Ser207Asp and Thr211Asp), and lacks the docking motif for substrate p38a (Enslen et al., 2000). In the context of full-length MEK6, the aspartic acid mutants confer activity toward its substrate p38a, as is the case for MEK1/2 (Huang et al., 1995). The turnover numbers for full-length MEK6/DD and wild-type doubly phosphorylated fulllength MEK6 are 12.8 ± 0.6 and 8.0 ± 0.1, respectively (J.M.H. and E.J.G., unpublished data).

The structure was solved by single-wavelength anomalous dispersion (SAD) from a complete data set collected on a single selenomethionine-incorporated protein crystal and refined against 2.35 A ° resolution X-ray data. The final structure was refined in REFMAC5 (Murshudov et al., 1997) to an R factor of 19.6% (R_{free} 24.7%) with reasonable stereochemistry (Table 1). The protein crystallized in space group $P3_221$, with four subunits in the asymmetric unit. The four subunits form two tight dimers shown in Figure 1A (left panel). One of the two dimers is shown in the right panel of Figure 1A. The individual chains are very similar. In all the four chains, part of the activation loop (Val208–Cys216) is disordered. A TLS refinement was performed with four TLS parameters per chain (Painter and Merritt, 2006). The B factors were uniformly elevated, indicative of motion of the individual chains. Nevertheless, the pairwise root-meansquare deviation (rmsd) ranged between 0.6 and 0.8 A° among the four subunits. The model contains 1111 residues, 4 sulfate ions, and 331 water molecules.

The MEK6 Monomer Structure MEK6 belongs to the STE group of protein kinases (Manning and Davis, 2003), and the MEK6/DN/DD construct used is similar in length to another STE group kinase, TAO2 (TAO2 [1–320]), the structure of which was solved in an active conformation (Zhou et al., 2004). As with TAO2, the MEK6/DN/DD subunit adopts a bilobal fold, similar to other protein kinases (Jones et al., 1997; Knighton et al., 1991) (Figure 1B), with two additional helices (J and K) at the C terminus. The N-terminal lobe of MEK6/DN/DD is composed of a b sheet and one long helix (helix C); the C-terminal lobe is helical. Comparison of MEK6 to active TAO2 reveals dramatic differences, suggestive that MEK6 adopts an inactive structure despite the phosphomimetic mutations.

As in protein kinases generally, the N-terminal lobe b sheet of TAO2 consists of five strands (Figure 1B). (The first two strands of the b sheet are also referred to as the ATP phosphate binding ribbon, or P loop; Jones et al., 1997.) In contrast to TAO2, the phosphate binding ribbon in MEK6 is formed into a large loop between Ile56 and Glu68, reminiscent of an U loop (Leszczynski and Rose, 1986). At the C terminus of this U loop, Glu68 makes an ion pair with the catalytic lysine (Lys82) in b strand 3.

The activation loop of MEK6/DN/DD exhibits hallmarks of a kinase-inactive conformation. The DFG motif (subdomain VII) at the beginning of the activation loop adopts a modified DFGout configuration, which is present in some inactive kinases and inhibitor complexes (Wrobleski and Doweyko, 2005) (Figure 1B). Asp197 of the DFG occupies the pocket normally Figure 1A). The dimer brings the N termini of the two subunits together, creating an elongated ellipsoid (right panel of Figure 1A) that buries 1500 A ° $_2$ of surface. In the interface, the distorted U loop-shaped phosphate binding ribbon of one subunit binds in the ATP binding site of the opposite subunit (Figures 1B and 2A). Tyr64, which in active kinases is at the apex of the phosphate binding ribbon, occupies the nucleotide binding site of the opposite subunit. The backbone carbonyl groups of Tyr64 and Ala63 accept hydrogen bonds from the catalytic Lys82$_0$Nz ($_0$ denotes second subunit),

and the nitrogen atom in Val67 makes a hydrogen bond to the side-chain oxygen atom (Od1) in Asp206 in the activation loop. The U loop also make contacts with the opposite C terminus, where Leu59 contacts Leu332 (Figure 2A). Weak hydrogen bonds also link the U loop and the crossover connection at the back of the active site (not shown).

Overall, the interactions between the two subunits appear to both render the protein inactive and limit the accessibility of the activation loop phosphorylation sites (blue spheres in Figure 1A) toward other kinases or phosphatases.

The dimer interface also involves the linker between b strand 3 and helix C and the loop between b strand 4 and b strand 5 (Figure 2A). An unusual ''arginine stack'' is found in the center of this interaction (Figure 2B). Arg83, which is located at the end of b strand 3, stacks with its symmetry mate. This arginine stack is stabilized by ion-pair interactions with Asp124 from the loop between b strand 4 and b strand 5 of the opposite subunit (and the symmetry-related interaction between Arg83 and Asp124).

Arginine stacks are rare in protein structures but are thought to stabilize interactions (Magalhaes et al., 1994). An arginine stack very similar to this one was recently found to be involved in the synaptotagmin switch mechanism (Fuson et al., 2007).

MEK6 Oligomerization in Solution

To obtain information on the molecular envelope and state of oligomerization in solution, SAXS was performed on MEK6/DN/ DD at the SIBYLS beamline at the Advanced Light Source (Putnam et al., 2007; Tsutakawa et al., 2007). The shape of the scattering curve and electron-pair distribution (Figures 3A and 3B) are consistent with an elongated ellipsoid (Koch et al., 2003).

The Guinier plots were linear, an indication of monodispersity of the sample (Figure 3C). The radius of gyration from the GNOM analysis was 38 A °. Based on the data below, the scattering vector q = 0.2 A° $^{-1}$, the Porod volume (hydrated volume) for MEK6/DN/DD is 132,000 A° ^{3}, providing an approximate molecular mass of 79,000 Daltons. The calculated molecular weight of each MEK6/DN/DD including the N-terminal hexa- His tag is approximately 36 kDa. Thus, the Porod volume is consistent with a dimer. Further, ab initio analysis in P1 symmetry by the program DAMMIN revealed an elongated structure (Figure 3D) of the same volume. The apparent P2 symmetry, when no symmetry was enforced, is again consistent with a dimer.

Both MEK6/DN/DD and full-length MEK6 also elute as dimers on a Superdex 75 16/60 gel-filtration column (elution volume _58 ml). ATP (1 mM) in the column buffer causes the elution volume to increase (Figure 4), as observed by analytical gel filtration through Superdex 200 10/300, suggestive of a change in the dimer-monomer equilibrium within a physiologically relevant concentration range (Gribble et al., 2000; Marjanovic et al., 1993).

The Sequence Conservation of the Subunit Interface

A multiple sequence alignment of MAP2Ks given in Figure 5A revealed that many residues in the observed MEK6 dimer are conserved in the MEK6/MEK3 subgroup, but are not conserved in MEK1/2. Tyr64, Arg83, Asp124, and Leu332 are conserved residues in the interface. Further, Tyr203, in the activation loop and interface, is conserved in the MEK3/6 subgroup. Single point mutations of the conserved residues (orange balls in Figure 1D) in the interface, including Arg83 involved in the arginine stack (discussed above), did not show any strong effect on the dimer.

A double mutant, D124A/W126S, was synthesized, which showed a slight change in the elution volume on a Superdex 200 10/300 gel-filtration column, indicative of a shift toward a monomer (Figure 4). We also tested the activity of these MEK6/ DN/DD mutants toward p38a and found that none of them rescued the low activity of MEK6/DN/DD (data not shown). These data further support the idea that the docking motif of MEK6 is required for activity toward its substrate MAPK (Bardwell, 2006).

Comparison of MEK6 with MEK1/2 Crystallographic studies of MEK1/2 were on inactive, unphosphorylated MEK1/2 (Ohren et al., 2004). There are several interesting parallels between

inactive MEK1/2 (N-terminal truncation mutant) and MEK6/DN/DD, however. First, there are similarities in secondary structure arrangements. The activation loops of both are formed into a small helix that makes most of its contacts with the N-terminal lobe, between the b sheet and helix C. The placement of Arg224 in the PYMAPER sequence is similar in both structures, in close proximity to the phosphorylation sites in active kinases (Figure 1D). In MEK1/2, the loop following the PYMAPER sequence is shorter by three residues and not quite as extended as in MEK6. At the C terminus, MEK1/2 have very similar C-terminal helices (J and K). On the other hand, MEK1/2 have a normal phosphate binding ribbon, in contrast to the U loop observed in MEK6/DN/DD.

A second similarity is that both MEK6 and MEK1/2 form dimers. However, the dimers are mediated by completely different contacts (Figure 5B). In MEK6, most of the interactions are between the N-terminal domains, as discussed above, whereas in MEK1/2, the interface is near helix G and the activation loop. Further, the MEK6 dimer adopts an antiparallel configuration, whereas MEK1/2 form a parallel configuration. Residues that form the interfaces are conserved in each subgroup (Figure 5A) but not between subgroups. In the MEK1/2 dimers, access to the active site is blocked for macromolecules, although not for small molecules. Further access to the activation loop by macromolecules is also partially restricted in MEK1/2. These data suggest similar roles for the MEK1/2 and MEK6 dimers in regulation of their activity and phosphorylation site processing by kinases and phosphatases.

DISCUSSION

Recent structural studies have revealed that many protein kinases form distinctive higher-order assemblies with altered activities. For example, two recent studies, one on EGFR (Zhang et al., 2006) and the another on antiviral protein kinase PKR (Dey et al., 2005), implicate dimerization in the activation mechanism.

Our data suggest that MEK6 forms an autoinhibitory dimer in the absence of its own substrates or other interacting partners. The elongated ellipsoidal dimer observed crystallographically for MEK6/DN/DD was also found for full-length wild-type MEK6 in SAXS analysis, showing that the dimer is a feature of full-length MEK6. The primary function of the autoinhibitory dimer may be to maintain MEK6 in an inactive form in the absence of its substrates. So far, it is unclear how the dimer is broken by substrate interactions. The dimer may also have a role in restricting the activation of MEK6. The MEK6 activation loop, although partially disordered, is surrounded by protein and is inaccessible to macromolecules. The docking motif (DVD motif) for MAP3Ks identified by Takekawa et al. (2005) is at the C terminus of MEK6.

Because the C-terminal residue Leu332 is in the dimer interface, it is apparent that interactions with a MAP3K should disrupt the MEK6 dimer, thus perhaps making the activation loop of MEK6 more available for processing by MAP3K. Thus, it is possible that this inactive dimer has a role both in the phosphorylated and unphosphorylated forms. In the active phosphorylated form, it restricts access to inappropriate substrates. In the unphosphorylated form, it prevents activation by inappropriate kinases.

It is interesting that MEK1/2/DN, inhibitor bound and unphosphorylated, also form dimers. Although the interface is completely different from MEK6 (Ohren et al., 2004), the MEK1/2 dimers also block access of the substrate binding site and the activation loop from macromolecules, perhaps again having a role in regulating both activity and activation. It is intriguing in this regard that in both MEK1/2 and MEK6, the phosphorylation sites are in the dimer interface but not visible in these inactive dimers. Because the MEK1/2 study was done on unphosphorylated MEK1/2 and our study was done with phosphorylation site mimetics, apparently the stability of the dimers may not depend on phosphorylation status in either case.

This autoinhibitory dimer of MEK6, and by inference MEK1/2 dimers, add to a growing list of unanticipated allosteric regulatory mechanisms that confer pathway specificity in MAP kinase modules and other protein kinases (Goldsmith et al., 2007; Biondi and Nebreda, 2003). Crystal structural studies from several laboratories, including ours, previously showed that the docking

interaction between MAP2Ks and MAPKs works allosterically to make the activation loop of MAPKs available for processing by kinases and phosphatases (Chang et al., 2002; Zhou et al., 2006). Here we see that MAP2K adopts an inactive configuration in the absence of its substrates, and again the activation loop is sequestered from the action of inappropriate kinases and phosphatases.

The autoinhibited dimer observed for MEK6 is also reminiscent of the phenomenon of autoinhibition in MAP3Ks mediated by regulatory domains (Takekawa et al., 2005). We look forward to more data on the significance of dimerization to the activity of MAP2Ks in the context of full-length wild-type proteins, and to fully exploring the role of individual residues in the dimer-monomer equilibrium.

EXPERIMENTAL PROCEDURES

Protein Expression and Crystallization

Human MEK6 (residues 45–334) was cloned into a pHisParallel vector using NcoI and SpeI sites (Sheffield et al., 1999). Point mutations Ser207Asp and Thr211Asp and others were introduced using a QuikChange kit (Stratagene). The MEK6/DN/DD protein was expressed in Rosetta 2 cells (Novagen). The cells were induced with 0.5mMIPTG at OD 0.7 and the protein was expressed for 12 hr at 18°C. Cells were lysed in two passes through an Avestin cell disruptor. The lysate was cleared by centrifugation at 35,000 3 g for 1 hr. The supernatant was applied to an Ni Sepharose column (GE Life Sciences) precharged with 0.1 M $NiSO_4$ and protein was eluted with 250 mM imidazole. The protein was further purified by anion-exchange chromatography on a MonoQ HR 5/5 column (GE Life Sciences) using a linear gradient and size exclusion chromatography on a Superdex 75 16/60 column (GE Life Sciences). The final buffer was 30 mM HEPES, 100 mM NaCl, 1 mM EDTA, 1 mM DTT, 1 mM TCEP (tris[2-carboxyethylphosphene]; Sigma). Protein was concentrated to 12 mg/ml using an Amicon concentrator. Prior to crystallization trials, 0.05% β-octyl glucoside was added. The selenomethionine-incorporated protein was expressed in met auxotrophic strain B834 (Novagen) grown in minimum media supplemented with selenomethionine and other nutrients (Doublie et al., 1994) and purified using the same protocol as the native protein. The crystals of both native protein and selenomethionine-incorporated protein were grown using the hanging-drop method. The well solution contained 1.6M Li_2SO_4 and 0.1 M Tris (pH 8.0). The crystals reached 0.2 3 0.2 3 0.15 mm in 1 week. The crystallization drop was supplemented with 20% glycerol and the crystals were frozen in liquid propane before data collection.

Data Collection and Structure Solution

A single-wavelength anomalous data set for the selenomethionineincorporated protein crystal was collected at beamline 19-BM at the Advanced Photon Source at Argonne National Laboratory. The data were integrated and scaled using the HKL2000 program (Otwinowski and Minor, 1997). Thirty-nine out of 48 possible selenomethionine sites were located using the program SHELXD (Schneider and Sheldrick, 2002). The phases were improved further by solvent flattening using the CNS program (Brunger et al., 1998). The initial model was constructed using a combination of manual tracing and Arp/ wARP auto tracing (Perrakis et al., 1999). The model was refined using the program REFMAC5 (Murshudov et al., 1997) in the CCP4 software suite (CCP, 1994), followed by iterative rounds of manual building with the program O (Jones et al., 1991). Within REFMAC5, rigid-body refinement was carried out separating the domains between Glu130 and Leu131 of the four monomers in the asymmetric unit. The final structure was refined to an R factor of 19.6% (Rfree 24.7%).

Small-Angle X-Ray Scattering

SAXS data were collected on MEK6/DN/DD, purified by gel filtration, on the SIBYLS beamline at the Advanced Light Source at Lawrence Berkeley National Laboratory with a Mar165 CCD detector. Scattering data were collected with 1.11587 A ° wavelength X-ray radiation, and processed by the Svergun software suite (Svergun et al., 2001). Three protein concentrations (10, 5, and 2.5 mg/ml) and the equivalent gel-filtration buffer were exposed for 7 and 70 s at room temperature. The program OGRE was used to subtract protein from buffer frames taken for the same length of exposure and account for the sample-detector distance and wavelength. Guinier analysis detected a small but significant radiation sensitivity that caused eventual sample aggregation, so only the first short exposure was used for analysis. The most concentrated sample, with the best signal-to-noise ratio, was superimposable on lower concentrations. These data were processed with PRIMUS of the ATSAS 2.1 suite (Svergun et al., 2001) for the Guinier and Porod analyses. These data were further processed using the regularization technique in GNOM, in which the pairwise electron distribution function (Patterson function) was obtained from the transform of the scattering function with a Dmax of 140 A °. Ten ab initio shape determination runs were done using DAMMIN (Svergun et al., 2001), which does not require input of the molecular mass and therefore is independent of user bias. The chi**2 from the DAMMIN log files (1.031– 1.033) reflect a good match of the individual ab initio shape predictions to the scattering curves. Averaged outputs of the ten runs were filtered using DAMAVER (Svergun et al., 2001). Models were superimposable with the observed DAMFILT shape shown in Figure 3D.

Kinase Assays

The phosphorylation of p38a and myelin basic protein (MBP) by various MEK6 enzymes was conducted using the standard [γ-^{32}P]ATP kinase assay conditions. All kinase assays were carried out under the standard conditions of 20 mM HEPES (pH 7.4), 20 mM MgCl2, 2.5 mM ATP, and substrate in a final volume of 100 ml at 30°C. For radiolabeled products, 5–10 mCi of [γ-^{32}P]ATP per reaction was mixed with the cold ATP. All reactions were initiated by the addition of enzyme after equilibration for 5 min at 30°C. Typical assays used 20 pmol of MEK6 and 2500 pmol of p38a or 2000 pmol of MBP. Assay termination and phosphorylation measurement were accomplished using protocols described previously (Braun et al., 1984; Racker, 1991). Reactions were terminated at desired time points by spotting aliquots on 3MM filter paper followed by immediate immersion in termination solution (10% trichloroacetic acid and 10 mM pyrophosphate). Washing with fresh termination solution was followed by autoradiography.

ACCESSION NUMBERS

The coordinates of MEK6/DN/DD have been deposited in the Protein DataBank under ID code 3ENM.

ACKNOWLEDGMENTS

We thank Diana Tomchick and Mischa Machius and the staff at Argonne National Laboratory for help in synchrotron data collection. We thank Luke Rice for help in analytical gel filtration. We thank beamline scientist Michal Hammel for aiding expert SAXS analysis. This research was supported by a grant from the NIH (DK46993) and funding I1128 and I1243 from the Welch Foundation. The U.S. Department of Energy, Office of Biological and Environmental Research, under contract number W-31-109-ENG-38, supported use of the Argonne National Laboratory Structural Biology Center beamlines at the Advanced Photon Source. X-ray scattering technologies at the Lawrence Berkeley National Laboratory SIBYLS beamline of the Advanced Light Source (ALS) are supported by the DOE program Integrated Diffraction Analysis Technologies (IDAT) under contract DE-AC02-05CH11231 with the U.S. Department of Energy. Applications of SAXS and crystallography at the

ALS relevant to human cancers are supported in part by National Cancer Institute grant CA92584.

REFERENCES

Bardwell, L. (2006). Mechanisms of MAPK signalling specificity. Biochem Soc. Trans. 34, 837–841

Bardwell, A.J., Abdollahi, M., and Bardwell, L. (2003). Docking sites on mitogen-activated protein kinase (MAPK) kinases, MAPK phosphatases and the Elk-1 transcription factor compete for MAPK binding and are crucial for enzymic activity. Biochem. J. 370, 1077–1085

Bellon, S., Fitzgibbon, M.J., Fox, T., Hsiao, H.M., and Wilson, K.P. (1999). The structure of phosphorylated p38g is monomeric and reveals a conserved activation-loop conformation. Structure 7, 1057–1065

Biondi, R.M., and Nebreda, A.R. (2003). Signalling specificity of Ser/Thr protein kinases through docking-site-mediated interactions. Biochem. J. 372, 1–13

Braun, S., Raymond, W.E., and Racker, E. (1984). Synthetic tyrosine polymers as substrates and inhibitors of tyrosine-specific protein kinases. J. Biol. Chem 259, 2051–2054

Brunger, A.T., Adams, P.D., Clore, G.M., DeLano, W.L., Gros, P., Grosse-Kunstleve, R.W., Jiang, J.S., Kuszewski, J., Nilges, M., Pannu, N.S., et al. (1998). Crystallography & NMR system: a new software suite for macromolecular structure determination. Acta Crystallogr. D Biol. Crystallogr. 54, 905–921

Canagarajah, B.J., Khokhlatchev, A., Cobb, M.H., and Goldsmith, E.J. (1997) Activation mechanism of the MAP kinase ERK2 by dual phosphorylation. Cell 90, 859–869

CCP4 (Collaborative Computing Project, Number 4) (1994). The CCP4 suite: programs for protein crystallography. Acta Crystallogr. D Biol. Crystallogr 50, 760–763

Chang, C.I., Xu, B.E., Akella, R., Cobb, M.H., and Goldsmith, E.J. (2002) Crystal structures of MAP kinase p38 complexed to the docking sites on its nuclear substrate MEF2A and activator MKK3b. Mol. Cell 9, 1241–1249

Chen, Z., Gibson, T.B., Robinson, F., Silvestro, L., Pearson, G., Xu, B., Wright, A., Vanderbilt, C., and Cobb, M.H. (2001). MAP kinases. Chem. Rev. 101, 2449–2476

DeLano, W.L. (2002). The PyMOL Molecular Graphics System (San Carlos, CA: DeLano Scientific)

Deng, Q., Liao, R., Wu, B.L., and Sun, P. (2004). High intensity ras signaling induces premature senescence by activating p38 pathway in primary human fibroblasts. J. Biol. Chem. 279, 1050–1059

Dey, M., Cao, C., Dar, A.C., Tamura, T., Ozato, K., Sicheri, F., and Dever, T.E (2005). Mechanistic link between PKR dimerization, autophosphorylation, and eIF2a substrate recognition. Cell 122, 901–913

Doublie, S., Xiang, S., Gilmore, C.J., and Carter, C.W., Jr. (1994). Overcoming non-isomorphism by phase permutation and likelihood scoring: solution of the TrpRS crystal structure. Acta Crystallogr. A 50, 164–182

Enslen, H., Brancho, D.M., and Davis, R.J. (2000). Molecular determinants that mediate selective activation of p38 MAP kinase isoforms. EMBO J. 19, 1301–1311

Fuson, K.L., Montes, M., Robert, J.J., and Sutton, R.B. (2007). Structure of human synaptotagmin 1 C2AB in the absence of Ca2+ reveals a novel domain association. Biochemistry 46, 13041–13048

Goldsmith, E.J., Akella, R., Min, X., Zhou, T., and Humphreys, J.M. (2007) Substrate and docking interactions in serine/threonine protein kinases Chem. Rev. 107, 5065–5081

Gribble, F.M., Loussouarn, G., Tucker, S.J., Zhao, C., Nichols, C.G., and Ashcroft, F.M. (2000). A novel method for measurement of submembrane ATP concentration. J. Biol. Chem. 275, 30046–30049

Han, J., Lee, J.D., Jiang, Y., Li, Z., Feng, L., and Ulevitch, R.J. (1996). Characterization of the structure and function of a novel MAP kinase kinase (MKK6). J Biol. Chem. 271, 2886–2891

Haystead, T.A., Dent, P., Wu, J., Haystead, C.M., and Sturgill, T.W. (1992) Ordered phosphorylation

of p42mapk by MAP kinase kinase. FEBS Lett 306, 17–22
Heo, Y.S., Kim, S.K., Seo, C.I., Kim, Y.K., Sung, B.J., Lee, H.S., Lee, J.I., Park, S.Y., Kim, J.H., Hwang, K.Y., et al. (2004). Structural basis for the selective inhibition of JNK1 by the scaffolding protein JIP1 and SP600125. EMBO J 23, 2185–2195
Huang, W., Kessler, D.S., and Erikson, R.L. (1995). Biochemical and biological analysis of Mek1 phosphorylation site mutants. Mol. Biol. Cell 6, 237–245
Hubbard, S.R. (1997). Crystal structure of the activated insulin receptor tyrosine kinase in complex with peptide substrate and ATP analog. EMBO J. 16, 5572–5581
Huse, M., and Kuriyan, J. (2002). The conformational plasticity of protein kinases. Cell 109, 275–282
Johnson, G.L., and Lapadat, R. (2002). Mitogen-activated protein kinase pathways mediated by ERK, JNK, and p38 protein kinases. Science 298, 1911–1912
Jones, T.A., Zou, J.Y., Cowan, S.W., and Kjeldgaard, M. (1991). Improved methods for building protein models in electron density maps and the location of errors in these models. Acta Crystallogr. A 47, 110–119.
Jones, G., Willett, P., Glen, R.C., Leach, A.R., and Taylor, R. (1997). Development and validation of a genetic algorithm for flexible docking. J. Mol. Biol 267, 727–748
Knighton, D.R., Zheng, J., Ten Eyck, L.F., Ashford, V.A., Xuong, N.-H., Taylor, S.S., and Sowadski, J.M. (1991). Crystal structure of the catalytic subunit of cyclic adenosine monophosphate-dependent protein kinase. Science 253, 407–413
Koch, M.H., Vachette, P., and Svergun, D.I. (2003). Small-angle scattering: a view on the properties, structures and structural changes of biological macromolecules in solution. Q. Rev. Biophys. 36, 147–227
Lei, M., Lu, W., Meng, W., Parrini, M.C., Eck, M.J., Mayer, B.J., and Harrison, S.C. (2000). Structure of PAK1 in an autoinhibited conformation reveals a multistage activation switch. Cell 102, 387–397
Leszczynski, J.F., and Rose, G.D. (1986). Loops in globular proteins: a novel category of secondary structure. Science 234, 849–855
Liu, S., Sun, J.P., Zhou, B., and Zhang, Z.Y. (2006). Structural basis of docking interactions between ERK2 and MAP kinase phosphatase 3. Proc. Natl. Acad Sci. USA 103, 5326–5331
Magalhaes, A., Maigret, B., Hoflack, J., Gomes, J.N., and Scheraga, H.A (1994). Contribution of unusual arginine-arginine short-range interactions to stabilization and recognition in proteins. J. Protein Chem. 13, 195–215
Manning, A.M., and Davis, R.J. (2003). Targeting JNK for therapeutic benefit: from junk to gold? Nat. Rev. Drug Discov. 2, 554–565
Marjanovic, M., Gregory, C., Ghosh, P., Willis, J.S., and Dawson, M.J. (1993) A comparison of effect of temperature on phosphorus metabolites, pH and Mg2+ in human and ground squirrel red cells. J. Physiol. 470, 559–574
Murshudov, G.N., Vagin, A.A., and Dodson, E.J. (1997). Refinement of macromolecular structures by the maximum-likelihood method. Acta Crystallogr. D Biol. Crystallogr. 53, 240–255
Nassar, N., Horn, G., Herrmann, C., Scherer, A., McCormick, F., and Wittinghofer, A. (1995). The 2.2 A ° crystal structure of the Ras-binding domain of the serine/threonine kinase c-Raf1 in complex with Rap1A and a GTP analogue. Nature 375, 554–560
Ohren, J.F., Chen, H., Pavlovsky, A., Whitehead, C., Zhang, E., Kuffa, P., Yan, C., McConnell, P., Spessard, C., Banotai, C., et al. (2004). Structures of human MAP kinase kinase 1 (MEK1) and MEK2 describe novel noncompetitive kinase inhibition. Nat. Struct. Mol. Biol. 11, 1192–1197
Otwinowski, Z., and Minor, W. (1997). Processing of X-ray diffraction data collected in oscillation mode. Methods Enzymol. 276, 307–326
Painter, J., and Merritt, E.A. (2006). Optimal description of a protein structure in terms of multiple groups undergoing TLS motion. Acta Crystallogr. D Biol. Crystallogr. 62, 439–450
Pearson, G., Robinson, F., Beers Gibson, T., Xu, B.E., Karandikar, M., Berman, K., and Cobb, M.H. (2001). Mitogen-activated protein (MAP) kinase pathways: regulation and physiological

functions. Endocr. Rev. 22, 153–183
Perrakis, A., Morris, R., and Lamzin, V.S. (1999). Automated protein model building combined with iterative structure refinement. Nat. Struct. Biol. 6, 458–463
Putnam, C.D., Hammel, M., Hura, G.L., and Tainer, J.A. (2007). X-ray solution scattering (SAXS) combined with crystallography and computation: defining accurate macromolecular structures, conformations and assemblies in solution. Q. Rev. Biophys. 40, 191–285
Racker, E. (1991). Use of synthetic amino acid polymers for assay of proteintyrosine and protein-serine kinases. Methods Enzymol. 200, 107–111
Raman, M., Chen, W., and Cobb, M.H. (2007). Differential regulation and properties of MAPKs. Oncogene 26, 3100–3112
Remenyi, A., Good, M.C., Bhattacharyya, R.P., and Lim, W.A. (2005). The role of docking interactions in mediating signaling input, output, and discrimination in the yeast MAPK network. Mol. Cell 20, 951–962
Schneider, T.R., and Sheldrick, G.M. (2002). Substructure solution with SHELXD. Acta Crystallogr. D Biol. Crystallogr. 58, 1772–1779
Sebolt-Leopold, J.S., and English, J.M. (2006). Mechanisms of drug inhibition of signalling molecules. Nature 441, 457–462
Sheffield, P., Garrard, S., and Derewenda, Z. (1999). Overcoming expression and purification problems of RhoGDI using a family of parallel expression vectors. Protein Expr. Purif. 15, 34–39
Svergun, D.I., Petoukhov, M.V., and Koch, M.H. (2001). Determination of domain structure of proteins from X-ray solution scattering. Biophys. J. 80, 2946–2953
Takekawa, M., Tatebayashi, K., and Saito, H. (2005). Conserved docking site is essential for activation of mammalian MAP kinase kinases by specific MAP kinase kinase kinases. Mol. Cell 18, 295–306
Tanoue, T., and Nishida, E. (2003). Molecular recognitions in the MAP kinase cascades. Cell. Signal. 15, 455–462
Tsutakawa, S.E., Hura, G.L., Frankel, K.A., Cooper, P.K., and Tainer, J.A (2007). Structural analysis of flexible proteins in solution by small angle X-ray scattering combined with crystallography. J. Struct. Biol. 158, 214–223
Wan, P.T., Garnett, M.J., Roe, S.M., Lee, S., Niculescu-Duvaz, D., Good, V.M., Jones, C.M., Marshall, C.J., Springer, C.J., Barford, D., and Marais, R. (2004) Mechanism of activation of the RAF-ERK signaling pathway by oncogenic mutations of B-RAF. Cell 116, 855–867.
Wang, X., and Tournier, C. (2006). Regulation of cellular functions by the ERK5 signalling pathway. Cell. Signal. 18, 753–760
Wang, Z., Harkins, P.C., Ulevitch, R.J., Han, J., Cobb, M.H., and Goldsmith, E.J. (1997). The structure of mitogen-activated protein kinase p38 at 2.1-A° resolution. Proc. Natl. Acad. Sci. USA 94, 2327–2332
Wrobleski, S.T., and Doweyko, A.M. (2005). Structural comparison of p38 inhibitor-protein complexes: a review of recent p38 inhibitors having unique binding interactions. Curr. Top. Med. Chem. 5, 1005–1016
Xie, X., Gu, Y., Fox, T., Coll, J.T., Fleming, M.A., Markland, W., Caron, P.R., Wilson, K.P., and Su, M.S. (1998). Crystal structure of JNK3: a kinase implicated in neuronal apoptosis. Structure 6, 983–991
Yoon, S., and Seger, R. (2006). The extracellular signal-regulated kinase: multiple substrates regulate diverse cellular functions. Growth Factors 24, 21–44
Zarubin, T., and Han, J. (2005). Activation and signaling of the p38 MAP kinase pathway. Cell Res. 15, 11–18
Zhang, F., Strand, A., Robbins, D., Cobb, M.H., and Goldsmith, E.J. (1994) Atomic structure of the MAP kinase ERK2 at 2.3 A° resolution. Nature 367, 704–711
Zhang, X., Gureasko, J., Shen, K., Cole, P.A., and Kuriyan, J. (2006). An allosteric mechanism for activation of the kinase domain of epidermal growth factor receptor. Cell 125, 1137–1149

Zhou, T., Raman, M., Gao, Y., Earnest, S., Chen, Z., Machius, M., Cobb, M.H., and Goldsmith, E.J. (2004). Crystal structure of the TAO2 kinase domain: activation and specificity of a Ste20p MAP3K. Structure 12, 1891–1900

Zhou, T., Sun, L., Humphreys, J., and Goldsmith, E.J. (2006). Docking interactions induce exposure of activation loop in the MAP kinase ERK2. Structure 14, 1011–1019

Table 1. Statistics of Crystallographic Data and Refinement

Space group	$P3_221$
Unit cell dimensions (Å)	$a = b = 122.66$, $c = 195.54$
Wavelength (Å)	0.97905
Resolution (Å)	20–2.35
Number of unique reflections	71,376
Average multiplicity (last shell)	6.6 (6.4)
Completeness (%) (last shell)	99.9 (99.9)
Intensity I/σI (%)	35/1.7
R_{sym} (last shell)[a]	0.07 (0.68)
R_{work}/R_{free}[b]	0.206/0.257
Nonhydrogen protein atoms	8,835
Waters	331
Rmsd in bond length (Å)[c]	0.02
Rmsd in bond angles (°)[c]	2.00
Average B values (Å^2)	57.2
Ramachandran plot statistics (%)	
Residues in most favored region	89.1
Residues in additionally allowed region	9.1
Residues in generously allowed region	1.8
Residues in disallowed region	0.0

[a] $R_{sym} = \sum|I_{avg} - I_j|/\sum I_j$.

[b] R factor = $\sum|F_o - F_c|/\sum F_o$, where F_o and F_c are observed and calculated structure factors, respectively, R_{free} was calculated from a randomly chosen 5% of reflections excluded from the refinement, and R_{work} was calculated from the remaining 95% of reflections.

[c] Rmsd is the root-mean-square deviation from ideal geometry.

Figure 1. The Structure of MEK6/DN/DD
(A) The left panel shows the two dimers in the asymmetric unit; the right panel shows one of the crystallographic dimers. The two monomers are in yellow and pink. The disordered activation loop is shown as a dotted line.
(B) A monomer is depicted with the side chains of residues Glu68, Lys82, Asp99, Asp197, Phe198, and Tyr203 in ball and stick representation. The TAO2 structure in the same orientation is shown here for comparison. The red box highlights the U loop in MEK6/DN/DD and compares it with the b1 strand and the b2 strand enclosed in a red box in TAO2.
(C) Close-up view of the C terminus, helices J and K. Residues in the DVD motif are shown as blue spheres, His317, Thr322, Val324, Phe327, Val328, and Ile331. We mutated the residues in the dimer interface, Asp124, Tyr64, Arg83, Arg61, Leu59, and Tyr203 (shown as orange spheres) to alanine. Leu332 (green sphere) is in the DVD motif and was also mutated. Note that the second subunit of the dimer is nearby (in yellow).
(D) Close-up view of the activation loop and PYMAPER loop in the same color scheme as in (A). Arg178, Asp179, Lys181, Pro218, Tyr219, Leu229, and Arg224. Drawn in PyMOL (DeLano, 2002).

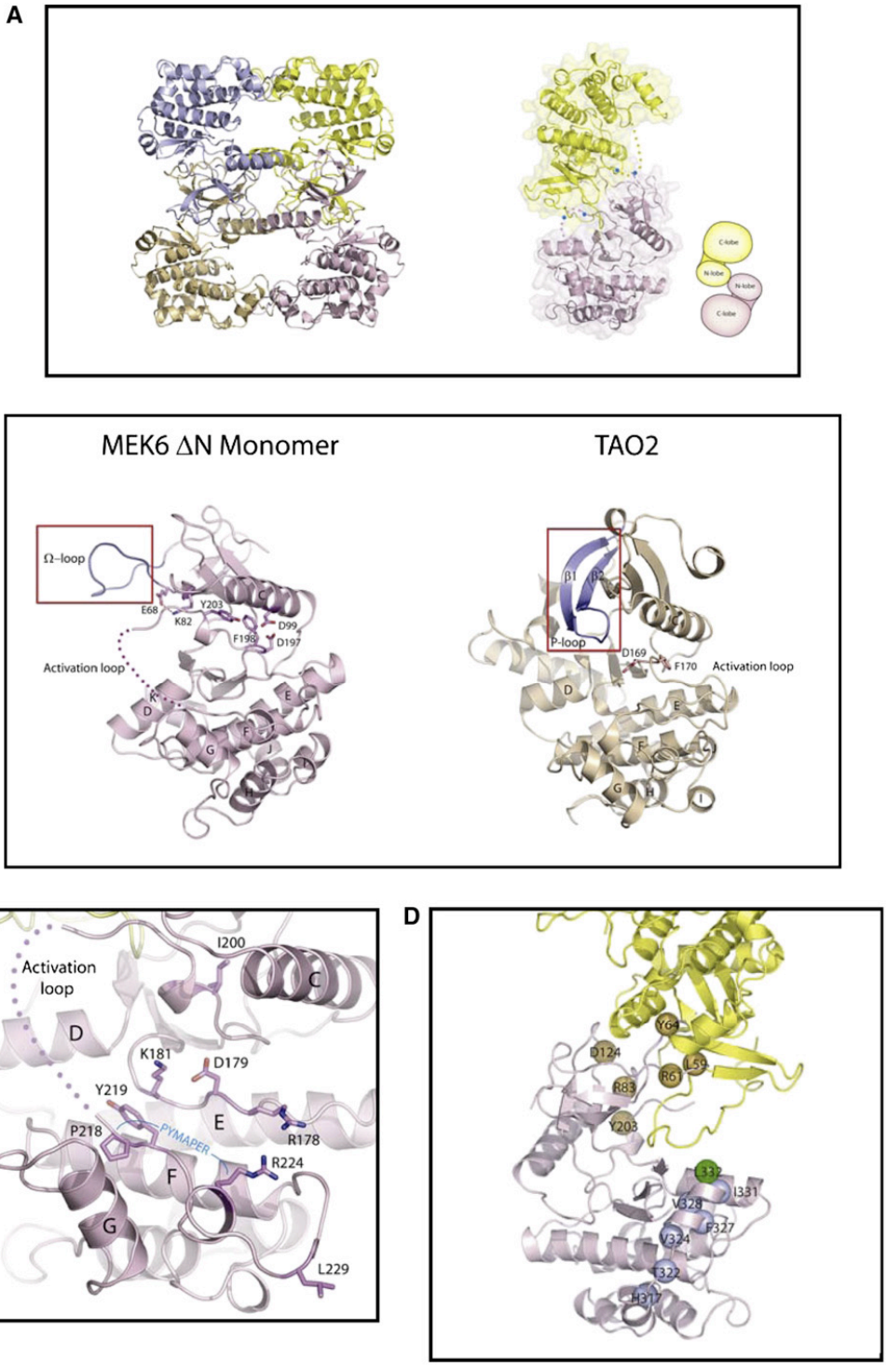

Figure 2. The Dimer Interface (A) Stereo view of the two U loops bound to the opposite subunit active sites, and contacts with the C terminus. Two subunits are shown, and rendered in cartoon. Side chains of Leu59, Arg61, Tyr64, and Leu332, and the backbone of Gly60 and Arg61, are rendered for both monomers. Dotted lines denote hydrogen bonds (2.8– 3.0 A °). (B) View of a 180_ rotation about Y from (A) showing the arginine stack. Arg83, Ala86, Asp124, and Trp126 are rendered in ball and stick representation. Electron density contoured at 1s covers selected side chains.

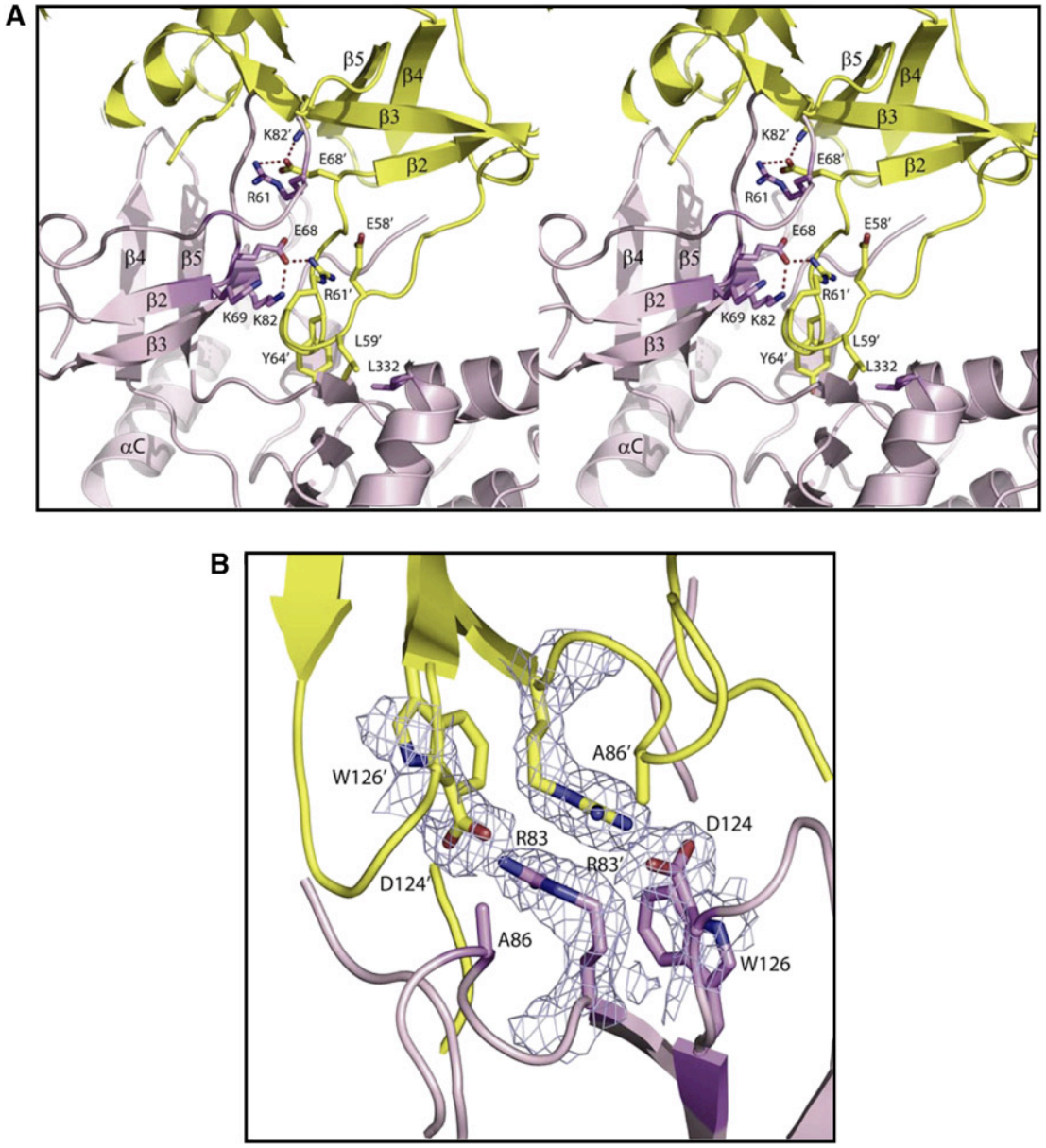

Figure 3. Low-Angle X-Ray Scattering of MEK6/DN/DD (A) Buffer-subtracted scattering profile (black) of MEK6/DN/DD is consistent with an extended conformation. The fit to the experimental data of one ab initio DAMMIN model is shown in red. (B) The electron-pair distribution function of the experimental data shows a general bell-shaped curve, but with an asymmetric bias toward the longer distances, indicating an extended structure. Dmax was 140 A ° . (C) Data in the Guinier region are linear, indicating monodispersity of the sample in solution. (D) Averaged and filtered ab initio shape prediction for MEK6/DN/DD in solution was calculated by the program DAMMIN and aligned using the DAMAVER program suite. The overall volume is consistent with two molecules of MEK6/DN/DD and the crystallographically observed dimer.

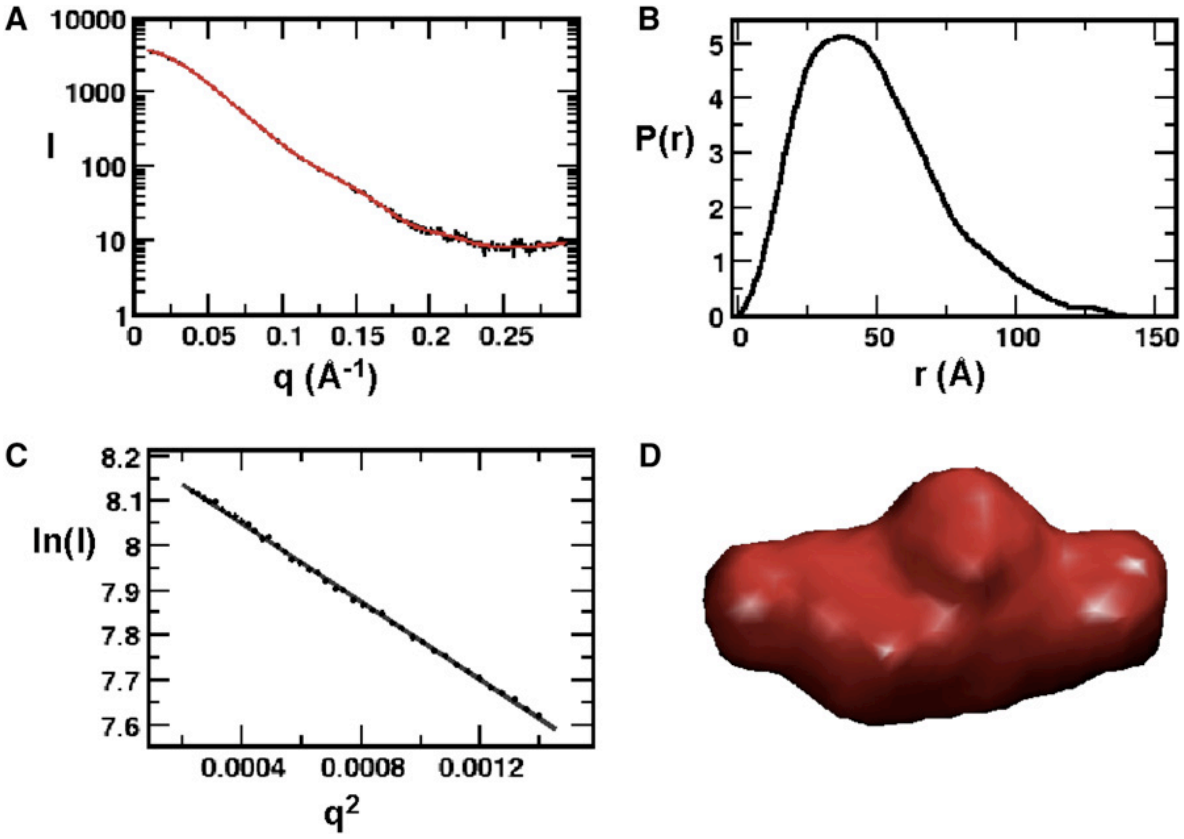

Figure 4. Analytical Gel Filtration of MEK6/ DN/DD Comparison of elution volumes from analytical gel filtration (Superdex 200 10/300) of MEK6/DN/DD in the presence (red) and absence (green) of ATP in the column buffer and a double mutant D124A/W126S (blue). A shift toward lower molecular weight in the presence of ATP and for the double mutant indicates a change in dimermonomer equilibrium.

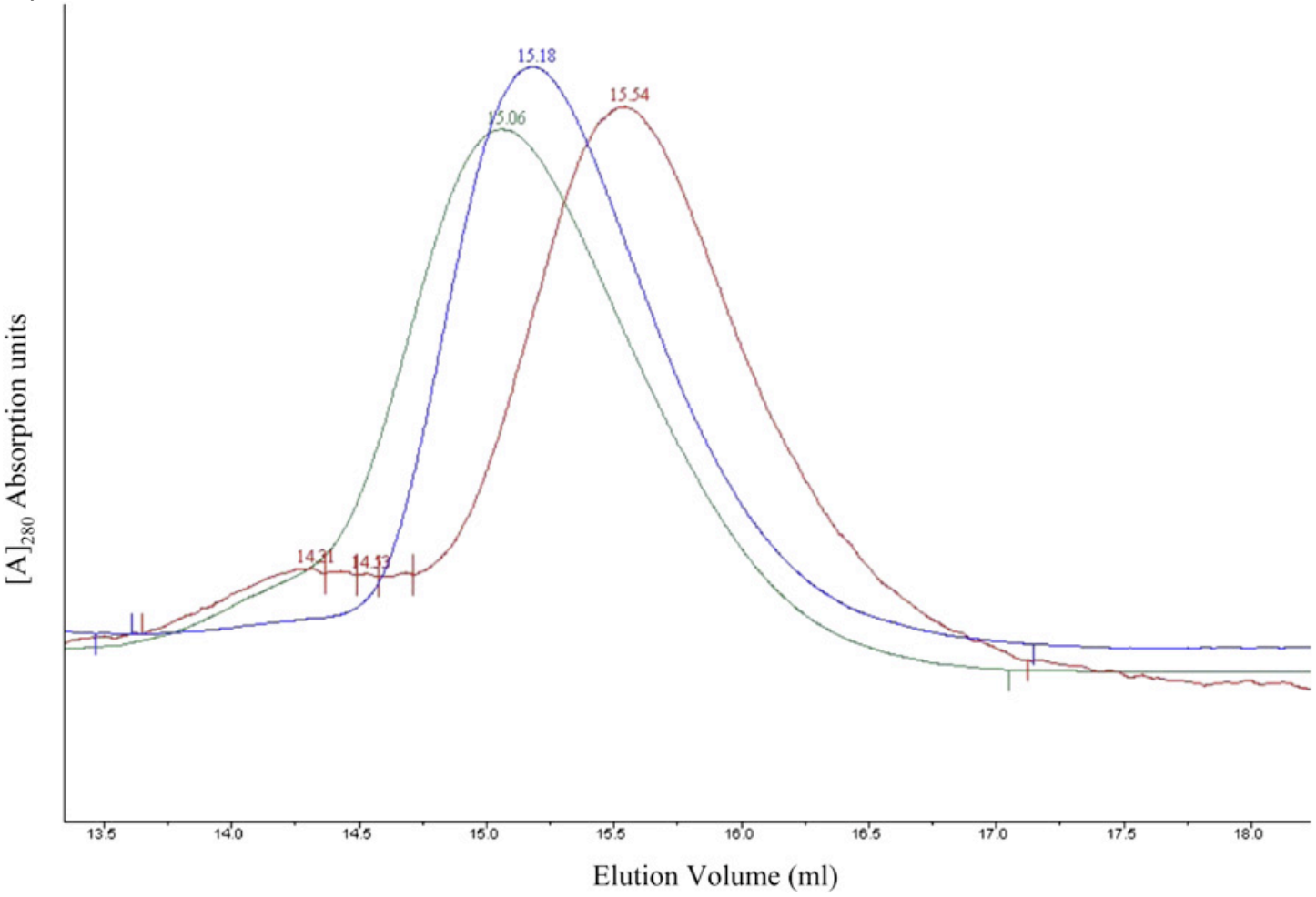

Figure 5. Comparison of Dimer Interface betweenMEK6andMEK1/2 (A) Sequence alignments of MAP2Ks in regions forming the dimer interfaces in MEK6 and MEK1/2. (B) The MEK6 (present work) and MEK1/2 (Ohren et al., 2004) (Protein Data Bank ID code IS9J) dimers are shown with the conserved residues rendered as balls. A cartoon representation shows the differences in packing of the dimers in the two MAP2Ks.

A

	^{60}		^{82}		^{123}		^{220}		^{277}
MEK6 Human	GRGAYG		KRIRAT		GDVW		MAPERINPELN		GTPFQ
MEK6 Mouse	GRGAYG		KRIRAT		GDVW		MAPERINPELN		GTPFQ
MEK3 Human	GRGAYG		KRIRAT		GDVW		MAPERINPELN		GTPFQ
MEK3 Mouse	GRGAYG		KRIRAT		GDVW		MAPERINPELN		GTPFQ
MEK4 Human	GRGAYG		KRIRST		GDCW		MAPERIDPSAS		NSVFD
MEK4 Mouse	GRGAYG		KRIRST		GDCW		MAPERIDPSAS		NSVFD
	^{75}		^{97}		^{137}		^{231}		^{308}
MEK1 Human	GAGNGG		KLIHLE		GEIS		MSPER---LQG		MAIFE
MEK1 Mouse	GAGNGG		KLIHLE		GEIS		MSPER---LQG		MAIFE
MEK1 Rat	GAGNGG		KLIHLE		GEIS		MSPER---LQG		MAIFE
MEK2 Human	GAGNGG		KLIHLE		GEIS		MSPER---LQG		MAIFE
MEK2 Mouse	GAGNGG		KLIHLE		GEIS		MSPER---LQG		MAIFE
MEK2 Rat	GAGNGG		KLIHLE		GEIS		MSPER---LQG		MAIFE
MEK5 Human	GAGNGG		KLIHLE		GEIS		MSPER---ISG		LMPLQ
MEK5 Mouse	GAGNGG		KLIHLE		GEIS		MSPER---ISG		LMPLQ
MEK5 Rat	GAGNGG		KLIHLE		GEIS		MSPER---ISG		LMPLQ

B